RSC Advances

PAPER

View Article Online
View Journal | View Issue

Cite this: *RSC Adv.*, 2025, **15**, 6474

Environmental innovation: polyaniline–cuttlebone nanocomposite as a potent antimicrobial agent and a synergistic barrier against doxorubicin-induced toxicity

Esraa Salama,[a] Fatma I. Abo El-Ela,[b] Walid Hamdy Hassan,[c] Ahmed A. Farghali,[d] Abdullah A. Eweis,[e] Sarah H. M. Hafez[f] and Rehab Mahmoud *[g]

This work emphasizes the importance of utilizing cuttlebone waste as a sustainable solution for waste management and the development of antimicrobial materials by incorporating it as a supporting phase for polyaniline (PANI) to form a nanocomposite. The three prepared materials were fully characterized using various techniques, including FTIR, XRD, SEM, EDX for elemental analysis, Brunauer–Emmett–Teller (BET) surface area measurements, particle size distribution analysis, and zeta potential measurements. The study focuses on the development of novel molecules with potential antibacterial and antifungal activity against clinical pathogens responsible for infectious diseases. The antibacterial and antifungal activities of the polyaniline/cuttlebone (PANI/CB) composite were evaluated using methods such as minimum inhibitory concentration (MIC), minimum bactericidal concentration (MBC), and disk diffusion for bacterial samples, as well as MIC, minimum fungicidal concentration (MFC), antifungal percentage, and disk diffusion for fungal samples. Notably, the PANI/CB composite exhibited a distinct crystallite size and characteristic XRD pattern, along with a significant BET surface area, demonstrating strong antimicrobial properties. Cuttlebone not only serves as a bioactive agent but also acts as a sustainable support to enhance the properties of polyaniline, forming a nanocomposite with a low MIC range (8–66 μg mL^{-1}) and effective action against Gram-positive bacteria such as *S. aureus*, although it showed less susceptibility against Gram-negative bacteria like *E. coli*. The MTT assay results demonstrated that while PANI and CB alone exhibited minimal cytotoxicity on Huh7 cells, the combination of doxorubicin (DOX) with PANI/CB significantly enhanced the cytotoxic effect, suggesting a synergistic interaction that could improve the therapeutic efficacy of DOX. Additionally, the effectiveness of the polyaniline/cuttlebone composite in protecting against DOX-induced hepatic and renal damage in rats was evaluated. Tissue damage was assessed using serum markers such as alanine transaminase (ALT), aspartate transaminase (AST), urea, and creatinine. The results demonstrated a decrease in oxidative damage and significant improvements in liver and kidney function markers in the polyaniline/cuttlebone-treated groups compared to those treated with individual components. Specifically, ALT levels decreased from 48 ± 2.8 IU L^{-1} to 21 ± 0.4 IU L^{-1}, AST from 195 ± 0.7 IU L^{-1} to 13 ± 1.08 IU L^{-1}, urea from 86 ± 1.4 mg dL^{-1} to 39 ± 0.7 mg dL^{-1}, and creatinine from 1.05 ± 0.03 mg dL^{-1} to 0.53 ± 0.01 mg dL^{-1}. These findings highlight the potential of utilizing cuttlebone waste as a sustainable material in antimicrobial applications, offering an eco-friendly solution for waste management while contributing to the development of potent antimicrobial nanocomposites.

Received 18th October 2024
Accepted 4th December 2024

DOI: 10.1039/d4ra07471h

rsc.li/rsc-advances

[a]*Chemistry Department, Faculty of Sciences, Beni-Suef University, Beni-Suef 62511, Egypt. E-mail: Esraa6salama96@gmail.com*

[b]*Department of Pharmacology, Faculty of Veterinary Medicine, Beni-Suef University, Beni-Suef 62511, Egypt. E-mail: Fatma.aboel3la@vet.bsu.edu.eg*

[c]*Department of Microbiology Mycology and Immunology, Faculty of Veterinary Medicine, Beni-Suef University, 62511 Beni-Suef, Egypt. E-mail: walidhamdyhassan@yahoo.com*

[d]*Department of Materials Science and Nanotechnology, Faculty of Postgraduate Studies for Advanced Sciences, Beni-Suef University, Beni-Suef 62511, Egypt. E-mail: ahmedfarghali74@yahoo.com*

[e]*Department of Botany and Microbiology, Faculty of Science, Beni-Suef University, Beni-Suef 62511, Egypt. E-mail: abdullah.ali@science.bsu.edu.eg*

[f]*Physics Department, Higher Technology Institute in New Heliopolis, Cairo, Egypt. E-mail: sarahafez789@gmail.com*

[g]*Chemistry Department, Faculty of Science, Beni-Suef University, Beni-Suef 62511, Egypt. E-mail: rehabkhaled@science.bsu.edu.eg*

1 Introduction

It is a public health priority to investigate and develop less expensive and more effective natural antimicrobial agents that have greater potential, minimal toxicity, good bioavailability, and fewer side effects than antibiotics, as microorganisms have developed an increasing resistance to antibiotics.[1] In addition, the escalating prevalence and development of multiple resistance mechanisms in microorganisms have significantly impacted the efficacy of conventional medications that are available in the market. Therefore, there is an ongoing requirement to identify novel pharmaceuticals with novel mechanisms of action in order to reduce these issues. Remarkably, nature has provided a fundamental and amazing source for the development of new and innovative pharmaceuticals from plants, animals, and microorganisms, which have exhibited remarkable structural diversity in the production of secondary metabolites.[2] This is due to antimicrobial resistance (AR), a process defined by microbial changes that cause antimicrobials to lose their potency and become ineffective against microbial diseases.[3] AR causes significant societal and economic harm and is one of the biggest threats to global health and food security. According to the World Health Organization, antibiotic resistance increases health risks and results in 700 000 deaths worldwide each year. Treatments for illnesses such as salmonellosis, gonorrhea, and pneumonia are challenged by AR.[4] The frequency of bacterial and fungal infections in animals and people, especially in those affected by wastewater, is a serious issue.

DOX is a commonly used and highly effective cytotoxic compound in the field of oncology. However, its use is limited by the risk of cardiotoxicity, which is directly related to the amount of the drug given. A thorough retrospective analysis found that approximately 7% of patients experienced congestive heart failure (CHF) as a result of doxorubicin treatment. This means that even though doxorubicin is one of the most widely prescribed and potent cytotoxic drugs, its use may be restricted due to the potential for progressive damage to the heart at higher doses, which could ultimately lead to CHF. As a result, patients who could benefit from continued doxorubicin therapy may be forced to stop using it and switch to a less effective alternative.[5]

The liver plays a crucial role in the human body by regulating important metabolic processes. Due to its unique location, the liver is exposed to a wide range of substances, such as alcohol, medications, and infectious agents, which can potentially harm its function. The liver is closely connected to the body's inflammatory response, which helps to combat harmful stimuli. However, chronic inflammation can lead to serious conditions like hepatic fibrosis, cirrhosis, and hepatocellular carcinoma (HCC). The link between inflammation and liver cancer can be explained through the inflammation-fibrosis-cancer continuum. HCC is a major cause of death worldwide. In advanced stages of the disease, chemotherapy is crucial to reduce the risk of recurrence after surgery.

Numerous researchers have proposed that the mechanism by which doxorubicin induces nephrotoxicity involves cellular impairment caused by the generation of an iron anthracycline free radical, which then damages the plasma membrane. The activity of angiotensin-converting enzyme (ACE) is crucial in the pathophysiology of arterial hypertension and nephrotoxicity. As a result, ACE inhibitors such as captopril are commonly used as antihypertensive medications and are believed to mitigate nephrotoxic effects. However, the role of ACE inhibitors in reducing doxorubicin-induced nephrotoxicity is still a topic of debate and is dependent on the specific type and mechanism of action. Some studies have suggested that ACE inhibitors may actually cause functional renal impairment, while others have found that captopril can partially inhibit the functional and morphological damage caused by doxorubicin. Given the ongoing discussions surrounding the impact of captopril as an ACE inhibitor on nephrotoxicity, further research is necessary to explore its potential as a free radical scavenger in the context of doxorubicin-induced nephrotoxicity.[6]

The discovery of antibacterial agents contributed to the extension of human life; however, their irrational application resulted in the development of bacterial resistance. Resistance is a global issue that is becoming more severe due to the excessive use or misuse of antibacterial medications in humans, animal husbandry, and agriculture.[7] Bacteria have developed resistance to the majority of the novel antibacterial agents that have been developed. Invasive bacterial infections are now more prevalent than they were at the beginning of the century, as the number of infections caused by pathogenic microorganisms that are resistant to the most recent or modern antibiotics is on the rise. The world's greatest threat to human health and existence is infectious diseases.[8] Public health initiatives neglect certain fungal infections, whether they are genuine pathogens or opportunists that contribute to the transmission of zoonoses. Consequently, additional prevention strategies are necessary.[9] Immunocompromised patients may experience a fatal outcome as a result of the elevated immune response that infected fungi were unable to adapt to the human host environment.[10]

Polyaniline (PANI) is one of the more commonly used conducting polymers because of its many advantages, including cheap monomers, simple polymerization, extended shelf life, and acid–base doping capabilities. Mainly employed against bacteria, fungi, and other microorganisms, PANI is an antibacterial agent.[11] Due to its conducting nature and tuneable chemical properties, PANI has been extensively studied as a conducting polymer for energy storage devices (ESDs), sensors, actuators, antistatic coating films, and antibacterial (AB) activity applications are examples of electrochemical-instruments.[12] In addition, the interior cartilaginous shell of octopuses, squid, and cuttlefish is called the cuttlebone (CB). CB powder has long been used as a medication to treat various ear illnesses prevent bleeding and enhance kidney function.[13] It is a naturally occurring source of biomaterial that may be powdered from the cuttlefish's chamber. Chitin and calcium carbonate (87.3–91.75%) represent the majority of CB's substance. Furthermore, it has trace amounts of copper, silicon, manganese, aluminum, titanium, and barium.[14] Biological

cuttlefish bone (CB) has already received a significant amount of attention, to improve the sustainability of the materials' production by utilizing economical secondary raw materials to stop resource depletion.[15] Since CB is an inorganic material, it may be calcined to create calcium oxide, which is useful for many applications (such as biomaterials for pharmaceuticals and bone implants).[16] These materials have potential uses in several practical domains, including energy and environmental applications.[17] Thus, the CB has been modified with the pyrolysis technique and has the potential to produce activated carbon/CaO, which is useful as a potential biomaterial[18]

Therefore, this current novel study aims at *in situ* generation and impregnation of PANI and CB as a homogeneous layer to examine whether such prepared material could potentially be used as a low-cost antimicrobial effective material. Analysis of zeta potentials, Fourier transform infrared (FTIR), X-ray diffraction (XRD), scanning electron microscopy with energy-dispersive X-ray (SEM-EDX), BET, and particle sizes were used to investigate the mechanism of the biomaterials and its surface structure.

2 Materials and methods

2.1. Chemicals

Sigma-Aldrich produced aniline (C_6H_7N, 99.7%), ammonium persulfate (APS, $(NH_4)_2S_2O_8$, 99.7%), and hydrochloric acid (HCl, 38%) for use in this study. The CB used was a byproduct of sepia officinalis supplied by a local fish shop in Egypt. CB was obtained from the Governorate of Alexandria, whereas potassium hydroxide (KOH) (Oxford, India) and sodium hydroxide (NaOH) were obtained from Egyptian Piochem for laboratory chemical use without further purification. Hydrochloric acid (HCl) was obtained from Carlo Erba reagents in Egypt. Methanol is provided by ALPHA CHEMIKA-India.

2.2. CB preparation

Cuttlefish bones from Alexandria Governorate Beach in Alexandria, Egypt, had been collected as marine trash. To remove the odor and microbes, the carbon black had to be extracted and divided into small parts. Following this, the carbon black was well-rinsed with deionized water, boiled for five minutes, and dried at 100 °C for 12 hours 67. The carbon black was pulverized into powder using a ball mill (photon ball mill). Following that, a five-hour pyrolysis technique was carried out in a tube furnace with a nitrogen atmosphere at 900 °C. Following the calcination process, the furnace was allowed to gradually return to the outside temperature. Before starting the analytical assessment, the specimens had been kept in a desiccator.

2.3. Preparation of PANI

PANI was prepared by the method of chemical oxidation polymerization. 1.6 mL aniline was added into the deionized water and stirred for half an hour with mixed solution. Then, 50 mL of the solution (HCl and ammonium persulfate concentration of 360 mM and 36.0 mM) was added dropwise into the aniline solutions. The aniline was polymerized for ~2 h at 0 °C. Then, methanol was used to remove oligomers in the PANI solution.

2.4. PANI/CB composite preparation

PANI/CB was fabricated by adding 1 g of PANI and 1 g of pyrolyzed CB to methanol. The mixture was stirred, then distilled water (25 mL: 25 mL) was added. After that, the mixture was dried at 60 °C for 12 hours to allow interaction between the two materials, as illustrated in Scheme 1 (the mass ratio of PANI/CB was approximately 1 : 1). The solid product of PANI/CB was then collected by vacuum filtration, washed multiple times, and dried at 60 °C (Scheme 1).

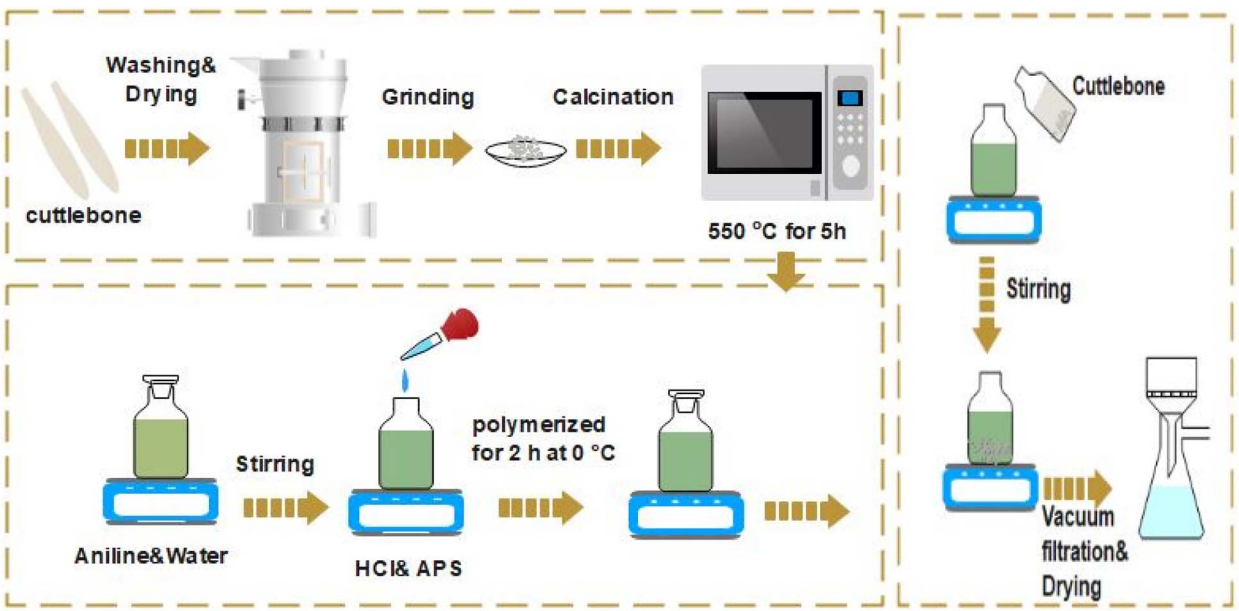

Scheme 1 Preparation of CB, and PANI/CB composite.

2.5. Estimation of antimicrobial activity of PANI, CB, and PANI/CB composite

2.5.1. Culture media. Mueller–Hinton agar, Sabouraud dextrose agar (SDA), Mueller–Hinton broth (SDB), and Sabouraud dextrose agar (MHL) culture media were obtained from Oxoid Laboratories in order to assess the biological efficacy of the manufactured substances. Next, in accordance with the instructions supplied by the creators, these culture media were created and utilized for the growth of bacteria and fungi.

2.5.2. Bacteria and fungi isolates. The bacterial strains for this study were obtained from the microbial culture repository of the Cairo Microbiology Research Center. These standard reference bacterial strains included several American Type Culture Collection (ATCC) authenticated microorganisms: *Staphylococcus aureus* (ATCC 25913), *Streptococcus pneumoniae* (ATCC 49619), *Listeria monocytogenes* (ATCC 19115), *Bacillus subtilis* (ATCC 35021), *Haemophilus influenzae* (ATCC 49766), and *Escherichia coli* (ATCC 25922). The fungal strains were sourced from the Fungal Research Institute in Doki, Giza, Egypt. The fungal collection comprised multiple species: *Aspergillus flavus* (RCMB 02783), *Aspergillus fumigatus* (RCMB 02564), *Aspergillus niger* (RCMB 02588), *Mucor indicus* (CNRMA 03.894), *Penicillium notatum* (NCPF 2881), and *Candida albicans* (RCMB 05035).

2.5.3. Preparing the inoculum for antifungal activity. Microbial suspensions were prepared from freshly cultured microorganisms. Fungal cultures were initially cultivated on Sabouraud dextrose agar, while bacterial cultures were grown on Mueller–Hinton agar plates. Bacterial cultures were incubated at 37 °C for 24 hours, and fungal cultures were maintained at 25 °C for five days. Using a sterile loop, 1–2 colonies were transferred to test tubes containing 5 mL of 0.9% saline solution. The suspensions were thoroughly homogenized by vigorous vortexing for 15 seconds. Inoculum standardization was performed using a barium sulfate suspension calibrated to the McFarland 0.5 standard. This standardization process ensured a precise microbial concentration of approximately 1.5×10^8 colony-forming units per milliliter (CFU mL^{-1}), providing a consistent and reproducible microbial inoculum for subsequent experimental procedures.

2.5.4. Agar disc diffusion assay for both anti-bacterial and fungal activity. The evaluation of the antimicrobial properties exhibited by the PANI, CB, and PANI/CB composite was determined by the bacterial and fungal strains using the agar disk diffusion technique. The strains of bacteria and fungi were evenly distributed on Mueller–Hinton agar (MHA) and Sabouraud dextrose agar (SDA) mediums, respectively. Sterile filter paper disks with a 6 mm diameter were added as a supplement. These disks were put on the agar plates after being loaded with different quantities of PANI, CB, and PANI/CB (1000, 500, 250, and 125 μg mL^{-1}). After that, the plates were incubated for five days at 25 °C and 37 °C for bacteria and fungus, respectively. During the antimicrobial susceptibility testing, a standardized methodology was employed to evaluate the inhibitory effects on various microorganisms. The experimental setup utilized 12 cm diameter Petri dishes, each containing two precisely positioned filter paper discs, with a microbial inoculum standardized to 1.5×10^8 Colony Forming Units per milliliter (CFU mL^{-1}). The comprehensive test panel included Gram-negative bacteria (*Escherichia coli* and *Haemophilus influenzae*), Gram-positive bacteria (*Streptococcus pneumoniae*, *Staphylococcus aureus*, *Bacillus subtilis*, and *Listeria monocytogenes*), and fungal strains (*Aspergillus flavus*, *A. fumigatus*, *A. niger*, *Mucor indicus*, *Penicillium notatum*, and *Candida albicans*). Conventional antibiotics cycloheximide and doxycycline served as reference standards to compare the efficacy of the test samples, with inhibition zone diameters carefully measured and recorded after the incubation period for subsequent detailed analysis.

2.5.5. The assay for minimum inhibitory concentration (MIC). The minimum inhibitory concentration (MIC) of PANI, CB, and the PANI/CB composite for the tested bacterial isolates was determined using the broth microdilution method. Various dilutions of each compound, ranging from 1000 to 0.97 μg mL^{-1}, were applied, with the bacterial concentration adjusted to 1.5×10^8 CFU mL^{-1}. This was then used in determining the MIC in Mueller–Hinton (LB) broth over a 24 hour incubation period. After incubation, visual inspection of the plates was performed to assess bacterial growth inhibition. The MIC was defined as the lowest concentration of PANI, CB, or PANI/CB composite that demonstrated visible inhibition of bacterial growth.

2.5.6. The MBC assay, or minimum bactericidal concentration. Following MIC determination of PANI, CB, and PANI/CB composite, 100 μL aliquots were collected from tubes showing no visible bacterial growth. These aliquots were then plated onto untreated Mueller–Hinton agar plates. The plates were incubated at 37 °C for 24 hours, and the Minimum Bactericidal Concentration (MBC) was established as the lowest concentration that completely prevented bacterial growth.

2.5.7. Fungal isolates: minimum inhibitory concentration assay (MIC-F). The MIC-F for fungal isolates were determined using the broth microdilution method. A 96-well microdilution plate with "U"-shaped bottom wells was prepared by adding 100 μL of Sabouraud Dextrose Broth (SDB) medium to each well. The first horizontal row was filled with 100 μL of test samples, followed by two-fold serial dilutions ranging from 1000 to 1.95 μg mL^{-1} by transferring 100 μL aliquots sequentially. Each well was then inoculated with 10 μL of fungal suspension, with individual columns representing different fungal strains. The experiment included cycloheximide as a reference antifungal agent, along with positive controls (medium without fungi) and negative controls (medium with fungi but without nanomaterials). The plates were incubated at 25 °C for 72 hours, after which growth was assessed visually by observing the formation of cell clusters or "buttons" in the wells. The MIC was defined as the lowest concentration showing visible inhibition of fungal growth.

2.5.8. The assay for minimum fungicidal concentration (MFC). To determine the minimum fungicidal concentration (MFC), 100 μL aliquots from wells containing PANI, CB, and PANI/CB composite at concentrations of MIC, MIC × 2, and MIC × 4 were subcultured onto Sabouraud dextrose agar (SDA) plates. The plates were incubated at 35 °C for 24–48 hours, and

MFC was evaluated against control growth. The MFC was defined as the lowest concentration that either completely inhibited yeast growth or resulted in fewer than three colony-forming units (CFUs), corresponding to 99.9% fungicidal activity.[19]

2.5.9. Sorbitol assay: impact of PANI, CB, and PANI/CB on diverse tested fungal strains' cell walls. To determine the possible mechanisms causing the antifungal effects of the test nanomaterials on various types of fungal cell walls, we carried out tests with and without sorbitol as a control, in culture media. 0.8 M sorbitol was added to the culture medium, which was a peptone–water medium, at a concentration of 15 g L^{-1}. The experiments were carried out utilizing the microdeletion technique on 96-well "U"-shaped plates. After that, the plates were aseptically sealed and incubated for five days at 25 °C before readings were taken. The higher MIC values noted in the medium containing sorbitol in comparison to the standard medium suggest that sorbitol, known for its ability to function as an osmotic protective agent in fungal cell walls, may indicate the cell wall as a potential target for the tested product.

2.5.10. Assay for antifungal activity. The antifungal activity assessment followed the methodology previously described by Agboola *et al.* Fungi were randomly selected and cultured on Sabouraud Dextrose Agar (SDA) at 35 °C for 72 hours. The fungal suspension was standardized to 1.5×10^8 Colony Forming Units (CFU) in 0.9% sodium chloride (NaCl) solution. The samples were combined with SDA at predetermined concentrations, autoclaved for 15 minutes at 121 °C, and maintained at 55 °C. Sterilized Petri plates were prepared with 20 mL of solidified Sabouraud dextrose agar medium, incorporating PANI, CB, and PANI/CB composite at concentrations of 1%, 2%, and 3%. Fungal growth was evaluated and analyzed after a 72 hour incubation period.

2.6. Cell viability on human hepatoma cell line (Huh7)

Huh7 cell line obtained from the Tissue Culture Unit at VACSERA in Giza, Egypt. This cell was seeded at a density of 1×10^4 cells per well in a 96-well plate and cultured in Dulbecco's Modified Eagle Medium (DMEM) that was enriched with sodium bicarbonate, supplemented with non-essential amino acids from Minimum Essential Medium (MEM), fortified with glutamine, and complemented with 10% heat-inactivated fetal bovine serum. The cell cultures were maintained under standardized laboratory conditions, specifically at a temperature of 37 °C within a controlled environment containing 5% carbon dioxide and maintained at high humidity for 12 hours. Following the initial incubation DOX, PANI, CB, PANI/CB composite and DOX + PANI/CB were introduced to the wells. After a 24 hour incubation period, the existing culture medium was carefully removed and replaced with 100 μL of fresh medium containing 10% (volume/volume) Cell Counting Kit-8 (CCK-8) reagent. The wells were then incubated for an additional hour. Cell viability was assessed by measuring the absorbance at 450 nm using a microplate reader, enabling precise calculation of cytotoxicity.

2.7. Experimental animals and housing conditions

The experimental study utilized forty-eight male Wistar rats, weighing between 120 and 150 g, sourced from the National Research Center's Animal House Colony in Cairo, Egypt. Prior to the study, the rats underwent a two-week quarantine to rule out any pre-existing microbial infections. They were housed in well-ventilated polypropylene cages with stainless steel tops, maintained at a temperature of 25 ± 5 °C and subjected to a 12 hour light–dark cycle. The rats were provided with unrestricted access to water and a standard, nutritionally complete pelleted diet. All experimental procedures were performed in strict compliance with the Experimental Animal Ethics Committee guidelines at Beni-Suef University, Egypt (Ethical Approval Number: BSU/FS/2014/10).

2.7.1. Experimental protocol. Adult Wistar rats were divided into five groups, each with 6 subjects. The groups were as follows:

(1) Normal group: these rats did not receive any treatment and served as the negative control.

(2) DOX-injected control: rats in this group were given DOX through intraperitoneal injection at a dosage of 2 mg per kg body weight once a week for 2 weeks, making them the positive control.

(3) DOX-injected animals treated with PANI: these rats received DOX through intraperitoneal injection (2 mg per kg body weight once a week) and were also given 120 mg of PANI/kg body weight daily through oral gavage for 2 weeks.

(4) DOX-injected animals treated with CB: rats in this group were given DOX through intraperitoneal injection (2 mg per kg body weight once a week) and were also given 140 mg of CB/kg body weight daily for 2 weeks.

(5) DOX-injected animals treated with composite (PANI/CB): rats in this group were given DOX through intraperitoneal injection (2 mg per kg body weight once a week) and were also given 140 mg of the composite/kg body weight daily for 2 weeks.

2.7.2. Serum analysis of ALT, AST, creatinine, and urea determination. After two weeks, the rats were anesthetized using diethyl ether inhalation. Blood samples were then promptly collected from the right jugular vein. The blood was allowed to coagulate and then centrifuged at 3000 rpm for 15 minutes. The resulting clear serum was stored at −30 °C for future biochemical analysis.

Kidney function (urea and creatinine)[20] and liver function (ALT and AST),[21] were measured according to the methods described.

2.8. Characterization of the prepared materials

XRD was carried out on a PANalytical (Empyrean) utilizing Cu Kα radiation (wavelength 0.154 nm) at an accelerating voltage of 40 kV and a current of 35 mA. FTIR spectra were obtained using a Bruker Vertex 70 (serial number 1341) to determine the molecular vibration in the chemical bonds. Scanning electron microscopy (SEM) images have been acquired using the JSM-IT200 to study the morphologies of the generated materials, while elemental analysis was performed using energy-dispersive X-ray (EDX) spectroscopy. The nitrogen adsorption desorption

isotherms were generated using Quantachrome TouchWin™ to explore the materials' surface area, average pore size, and mesoporosity.

3 Results and discussion

3.1. Characterization of prepared materials

3.1.1. The N_2 adsorption–desorption isotherms. The N_2 adsorption–desorption isotherms over the surface of the samples are depicted in Fig. 1A. Fig. 1B also shows the pore size distribution (PSD) curves. Table 1 summarizes the surface parameters acquired from the N_2 adsorption–desorption isotherms. The obtained isotherms of PANI, CB, and nanocomposite (PANI/CB) have IV isotherms with distinct hysteresis loops, which are typical of mesoporous structures. The three samples exhibit H_3 hysteresis loops, which can be described as the aggregation of plate-like particles with split-shaped pores[22] The CB has a greater surface area (92.64 $m^2\ g^{-1}$) than the PANI/CB (31.58 $m^2\ g^{-1}$). This decrease in surface area could happen as a result of the composite aggregation together, generating larger particles or structures. This aggregation can reduce the exposed surface area of the composite, resulting in a decrease in the BET surface area.[23]

3.1.2. Scanning electron microscopy (SEM). PANI, CB, and nanocomposite (PANI/CB) surface morphology were examined using scanning electron microscopy (SEM). Fig. 2A and B show PANI after polymerization, which has formed the structures. Agglomeration had clearly hidden the initial porous structure and stacked nanosheets.[24] On the other hand, Fig. 2C and D show SEM imaging of the structure of the CB. The particle size of CB was heterogeneous in nature and varied from fine to large-size flaky particles.[25] Fig. 2E and F show SEM imaging of the structure of the PANI/CB composite. From this Fig. 2, the two phases are easily identifiable. The first is the layered nanosheet form of PANI, and the second is the CB, which contains flakes. The added material can aggregate or cluster together, forming larger particles or structures.[26] This aggregation can reduce the exposed surface area available in the composite, resulting in a decrease in the BET surface area from 92.64 $m^2\ g^{-1}$ for the CB to 31.58 $m^2\ g^{-1}$ for the PANI/CB. The chemical composition of PANI, CB, and PANI/CB composites was identified using the EDX spectrum. According to the results, the PANI was composed of carbon (C), nitrogen (N), and oxygen (O) (Fig. 3A). Meanwhile, the CB powder was composed of carbon (C), oxygen (O), magnesium (Mg), calcium (Ca), phosphorus (P), zirconium (Zr), iodine(I), and titanium (Ti) (Fig. 3B), and the PANI/CB was composed of C, O, K, Ca, N, and Mg (Fig. 3C).

Table 1 Surface parameters for the samples

Sample	BET surface area ($m^2\ g^{-1}$)	Total volume in pores ($cm^3\ g^{-1}$)	Total area in pores ($m^2\ g^{-1}$)
CB	92.64	0.16	56.98
PANI	13.14	0.02	7.26
PANI/CB	31.58	0.06	20.47

3.1.3. Fourier-transform infrared (FTIR). Fig. 4 depicts the Fourier-transform infrared (FTIR) spectra of PANI, CB, and PANI/CB. The absorption peak of PANI at 3468 cm^{-1} is assigned to the stretching vibration of the amine, and bands found at 2340 cm^{-1} revealed hydrogen bonding. The peak at 1577 cm^{-1} is assigned to the stretching vibration of the aromatic ring. The peak at 1486 cm^{-1} is attributed to the N–H sharing vibration, and the peak at 1318 cm^{-1} is assigned to the C–N stretching vibration.[27] The FT-IR spectrum of CB is displayed in Fig. 4B; raw CB displayed weak OH and NH group absorption peaks in the range of 3651–3445 cm^{-1} due to the stretching vibration of water molecules.[25,28] Strong peaks at 1128, 885, and 702 cm^{-1} reveal the existence of aragonite structure carbonate groups n1, n2 (out-of-plane bend), and n4 (doublet C–O in plane bend), respectively.[29] A broad peak around 1441 cm^{-1} confirmed the n3-asymmetric stretch of the aragonite carbonate structure.[30]

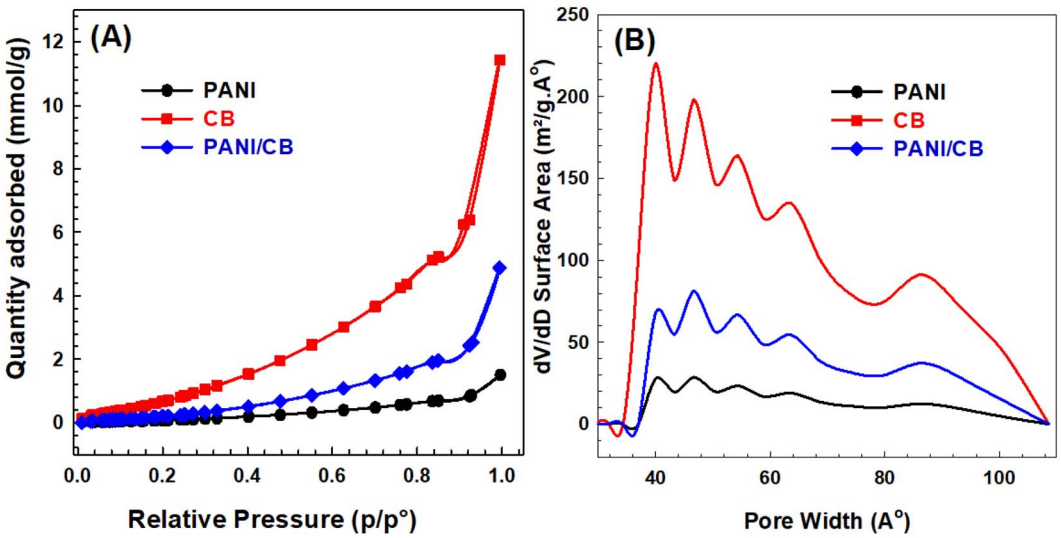

Fig. 1 (A) Adsorption–desorption isotherms of N_2, and (B) pore size distribution curves for the various samples understudy.

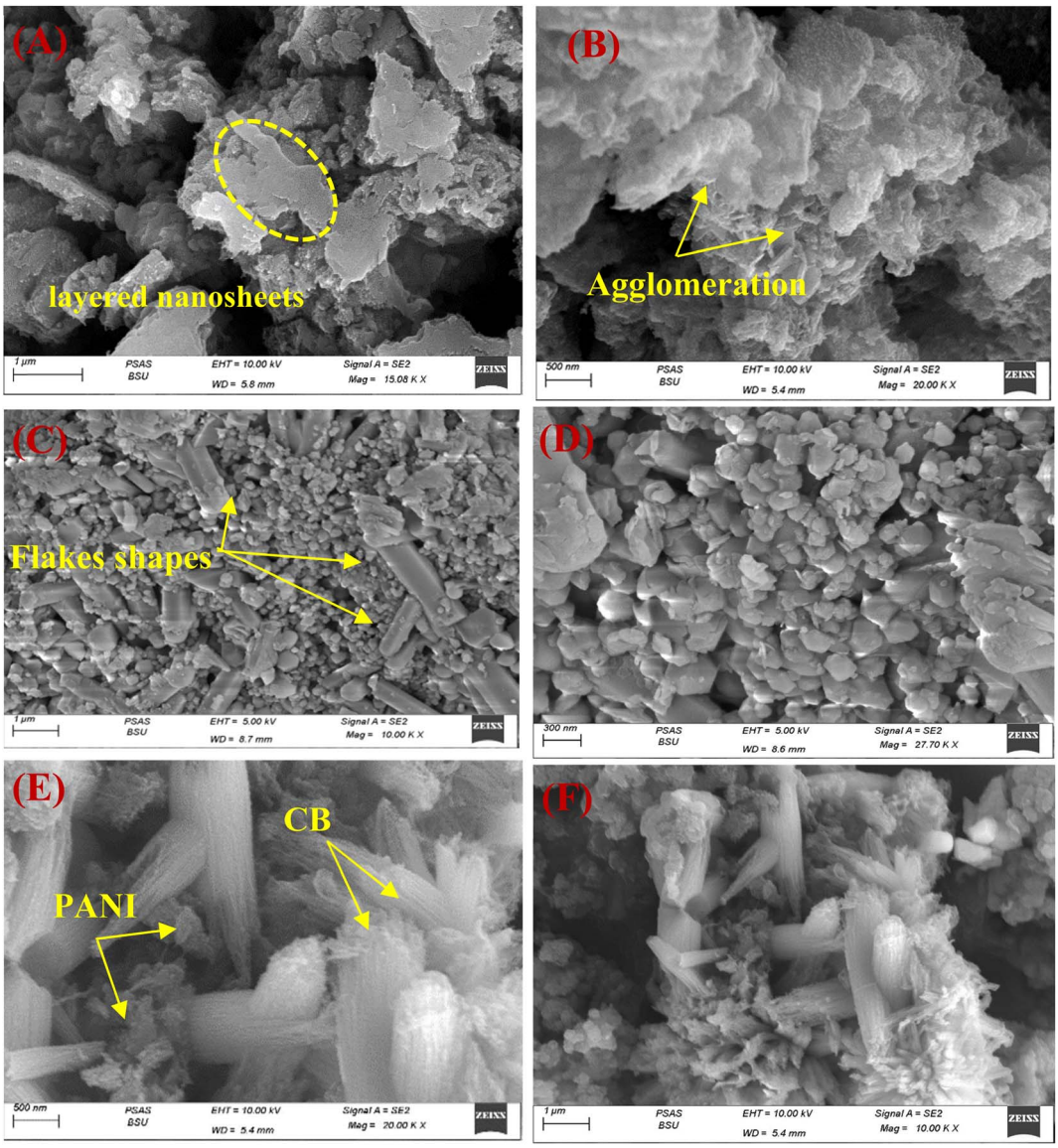

Fig. 2 SEM images of (A and B) CB, (C and D) PANI, and (E and F) PANI/CB composite.

The distinctive peaks detected in the FT-IR spectra of the PANI/CB nanocomposite provide vital information on PANI conformation in the CB channels and probable interactions between CB and PANI. The FT-IR spectrum of the PANI/CB nanocomposite (Fig. 4C) shows bands typical of both PANI and CB, confirming the existence of both components in the PANI/CB nanocomposite. Changes are clearly seen in all peaks; these changes are caused by the interaction of the constituents of the composite. This demonstrates that the CB interacts with the polymer matrix.[31]

Despite its low binding energy, the great importance of the hydrogen bond stems from its effects on the physical and chemical properties of the material, and is related to the degree of crystallinity, the regularity of the crystal system, and the absorbed water molecules bound. In general, a decrease in the intensity or a disappearance of a band involved in the H-bond interactions means that this interaction is an 'intermolecular' one, and *vice versa* for 'intramolecular' interactions. The FTIR study evidenced the intramolecular hydrogen bonding among the PANI/CB entities. The calculated hydrogen bond intensity was the ratio of the absorbance bands at 3468 and 3433 cm^{-1} (for the –OH peak) and 1318 and 1325 cm^{-1} (for the N–H peak) in PANI and PANI/CB respectively. The absorbance ratio showed an increase in the case of composite (1.05) more than that of PANI (1.03), indicating the hydrogen bonding interaction between the PANI and the interacted CB (Fig. 4).

3.1.4. X-ray diffraction (XRD). The XRD patterns of CB, PANI, and their composite are shown in Fig. 5. In the CB, the most significant peak is at around 30°, which corresponds to aragonite, while the other peaks indicate variable elements based on calcium carbonate. In essence, the CB's spectrum is quite similar to aragonite's diffraction pattern, with the (020), (110), and (113) planes showing the three strongest reflections.[28,32] CB particles have an influential diffraction peak plane

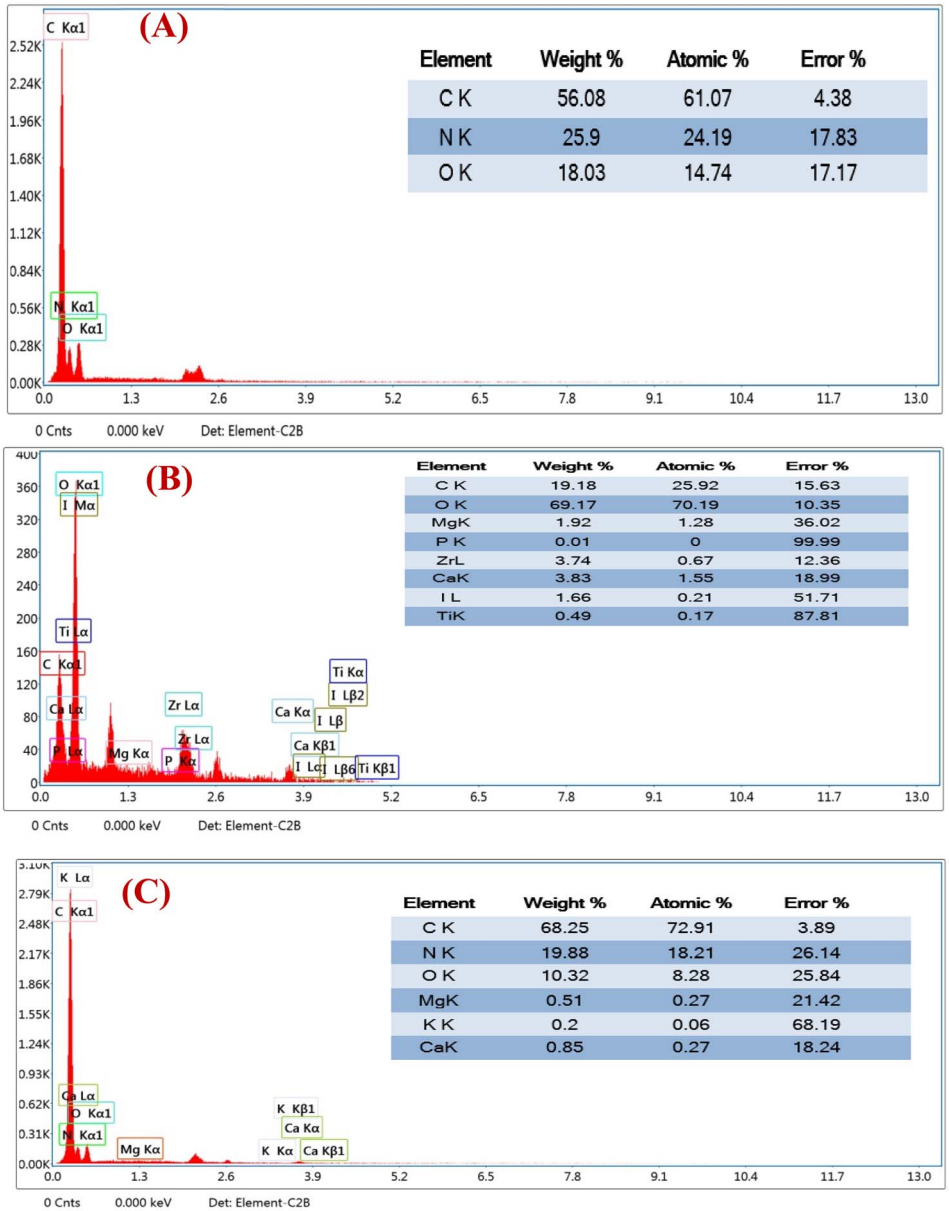

Fig. 3 EDX spectrum of (A) PANI, (B) CB, and (C) PANI/CB composite.

(104) typical of calcite polymorphs. The peak positions of PANI were well matched with the JCPDS card (#53-1891).[33,34] There is a small intense peak at $2\theta = 6.5°$, which is due to long PANI chains and a more ordered structure.[35] In PANI/CB, the broad peak centered at $2\theta = 27.2°$ with the plane of (003) appears, certifying the polymeric nature of PANI and PANI/CB composites. In PANI/CB diffraction peaks, all the peaks of PANI and CB are present without any impurity. It confirms the formation of PANI/CB composite with high purity. The crystallite size from the sharp peak (003) is calculated by Scherrer's equation,[36] and it is found to be 23.91 nm for PANI and 24.41 nm for PANI/CB composite, respectively. The increase in the intensity of XRD peaks in composite structure clearly suggests a strong interaction between the PANI backbone chain and the CB.[37]

3.1.5. Surface texture and 3D characterization. Surface morphology has been extensively studied because it can display vital properties, including deformations and heterogeneities that can affect the material's application. Mountain Map® 9.0 software was used to analyze the topographic SEM image. The surface profile analysis of PANI, CB, and PANI/CB reveals high roughness "peaks" and "valleys." Fig. 6 exhibits surface 3D SEM micrographs (left) and the Abbott–Firestone curve and the depth histogram of the samples (right). The height (or depth) distribution is characterized by a histogram, which implies the likelihood (frequency) of points being at a certain height (or depth). The Abbott–Firestone curve is marked in red, with the vertical axis graduated in depths and the horizontal axis in percentages of the overall population. The three samples have a distinct height distribution. The surface texture directions of

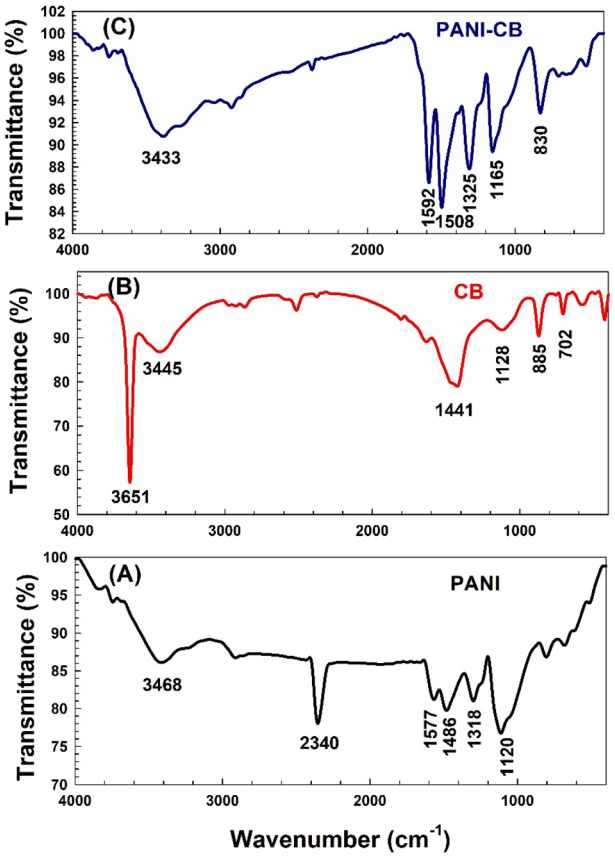

Fig. 4 FTIR spectrum of (A) PANI (B) CB (C) PANI/CB.

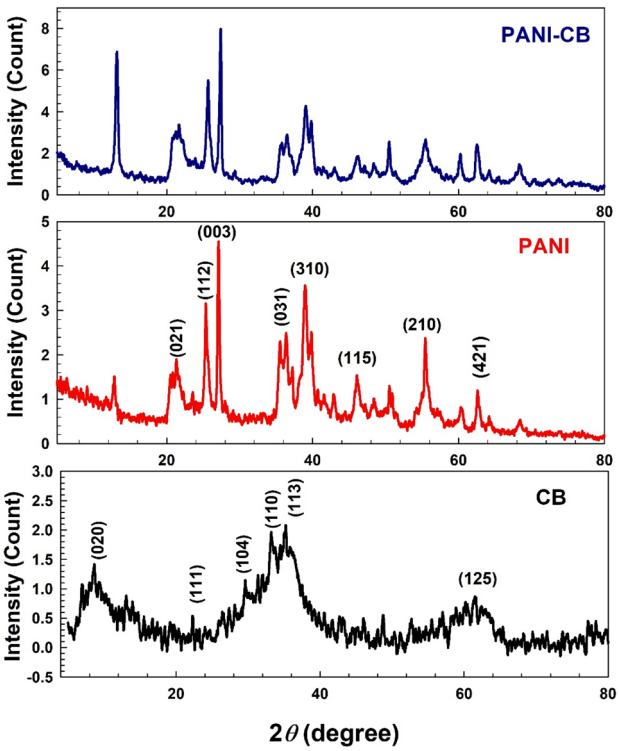

Fig. 5 XRD patterns of pure CB, PANI, and PANI/CB composite.

the samples were analyzed using Cartesian graphs (Fig. 7), as well as the related values of surface texture parameters, which may be associated with the inhomogeneity of the surface.[37] Table 2 shows the surface parameters in terms of roughness (R_a), roughness skewness (R_{sk}), roughness kurtosis (R_{ku}), and fractal dimension (D_f). The isotropy percentages of PANI, CB, and PANI/CB are 88.06, 83.12, and 95.98%, respectively. This is in line with the aspect ratio of the texture (Str) value of 0.676, 0.830, and 0.928, respectively, which indicates that the surface texture of the three samples is isotropic. If Str is close to the unit, the surface is isotropic, and if Str is close to 0, the surface is anisotropic.[38] The kurtosis and skewness parameters are processed using the square root of the surface height distribution (RMS). Roughness kurtosis (R_{ku}) is a measure of the "sharpness" of a surface and the unpredictability of profile heights. Spiky surfaces have $R_{ku} > 3$, bumpy surfaces have $R_{ku} < 3$, and absolutely random surfaces have $R_{ku} = 3$. Accordingly, the values of R_{ku} are 1.88, 2.916, and 2.608 for PANI, CB, and PANI/CB, respectively, which indicates the three samples have a rough surface. A roughness skewness (R_{sk}) value reflects the symmetry of the surface; a negative value implies a predominance of valleys, while a positive value indicates a "peaky" surface. PANI and PANI/CB have a positive R_{sk}, indicating that the surfaces of PANI and PANI/CB are peaky. Meanwhile, the CB has a negative value, indicating that the surface of the CB is a valley surface. The fractional dimension (D_f) quantifies the complexity of a fractal sample. The correlation coefficient (R^2) of the linear fit equal between the enclosed area and the scale of analysis, in this study was close to 1, indicating that the data were excellently fitted by linear functions. The values of D_f are 1.170, 1.418, and 1.109, as listed in Table 2. The creation of more regular structures is indicated by a decrease in D_f. The decrease in D_f indicates the formation of more regular structures.[39]

3.2. Antimicrobial activity investigation of the prepared materials

As illustrated in Table 3, the antimicrobial activity of PANI, CB, and their composite PANI/CB was evaluated against various microorganisms by determining the minimum inhibitory concentration (MIC) and minimum bactericidal concentration (MBC). For *Staphylococcus aureus*, PANI showed relatively high MIC and MBC values (27.33 ± 8 and 55 ± 15.55 μg mL^{-1}, respectively), while CB exhibited significantly lower values (MIC: 0.66 ± 0.288, MBC: 1.33 ± 0.57 μg mL^{-1}), indicating stronger antibacterial activity. The PANI/CB composite had intermediate MIC and MBC values (16 μg mL^{-1} for both), suggesting a synergistic effect but not as potent as CB alone. Similar trends were observed for *Streptococcus pneumoniae*, where CB had the lowest MIC and MBC values (0.833 ± 0.208 and 1.66 ± 0.57 μg mL^{-1}), while PANI/CB showed moderate activity compared to PANI, which had the highest values (MIC: 53.66 ± 14.6, MBC: 107.33 ± 29.22 μg mL^{-1}). For *Listeria monocytogenes*, the composite demonstrated better performance than PANI but was less effective than CB. In contrast, *Haemophilus influenzae* showed the best response to PANI/CB (MIC and MBC: 8 μg

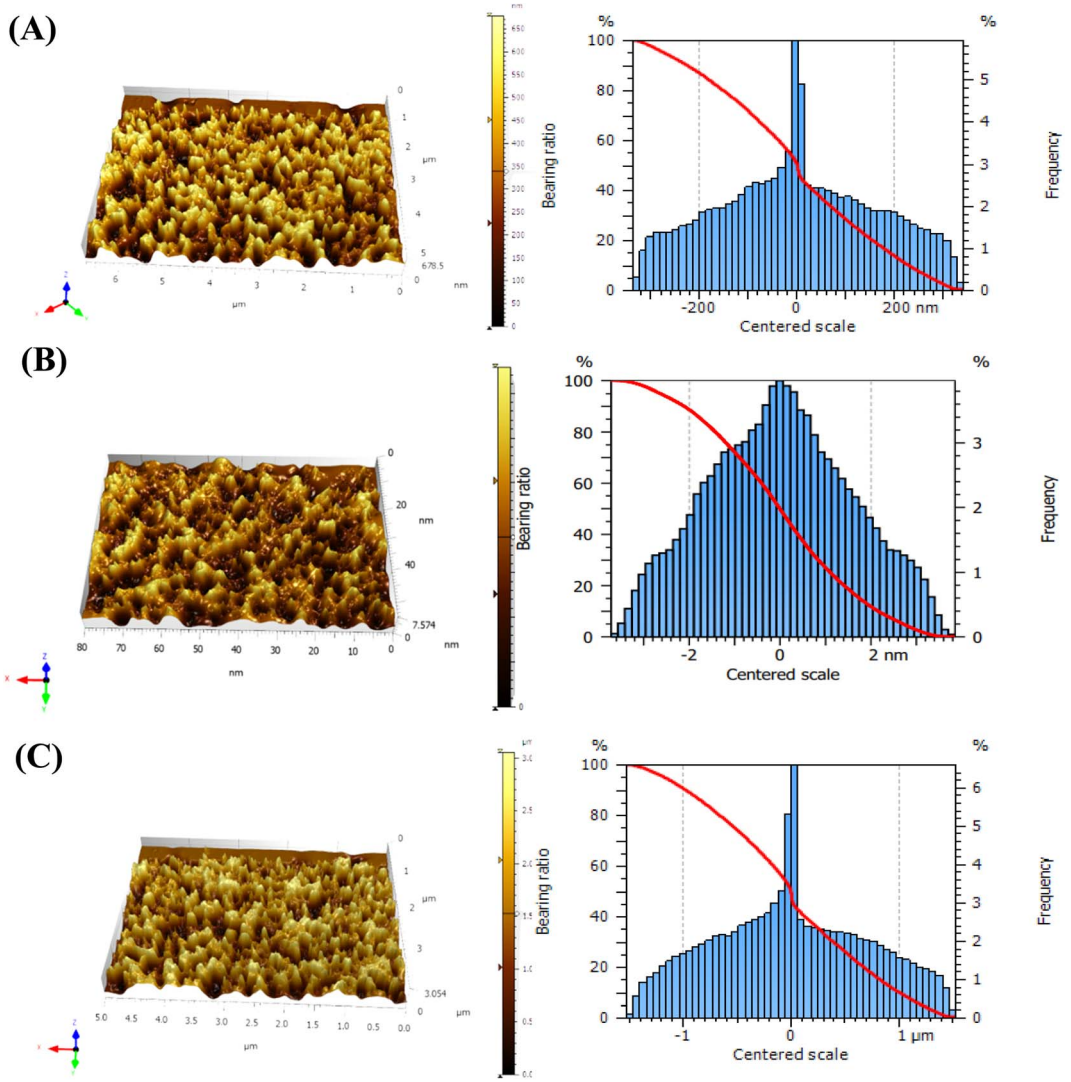

Fig. 6 Relevant 3-D SEM micrographs (left figure) and Abbotte–Firestone curve and the depth histogram (right figure) for (A) PANI, (B) CB, (C) PANI/CB.

mL^{-1}), while CB was the least effective with high MIC and MBC values (250 and 500 µg mL^{-1}). For *Bacillus subtilis*, CB exhibited moderate activity, while PANI/CB had a higher MIC of 66 µg mL^{-1} but matched the standard in terms of MBC (66 µg mL^{-1}). Lastly, for *Escherichia coli*, both PANI and PANI/CB demonstrated strong antibacterial effects with identical MIC and MBC values (6.66 ± 1.88 µg mL^{-1}), outperforming CB, which had much higher MIC and MBC values (500 µg mL^{-1}). Overall, CB generally exhibited stronger antibacterial properties across most microorganisms, while the PANI/CB composite often showed enhanced efficacy compared to PANI alone but not consistently superior to CB in all cases.

3.2.1. The zone of inhibition investigation. Fig. 8 demonstrated that, the comparative analysis of CB, PANI, and their composite treatments reveals distinct antimicrobial efficacy patterns across different bacterial strains and concentrations. CB showed strongest activity against Gram-positive bacteria, with maximum inhibition zones of 30.67 mm, 30.33 mm, and 29.67 mm for *S. aureus*, *S. pneumoniae*, and *L. monocytogenes*, respectively at 1000 µg mL^{-1}, while P treatment demonstrated higher efficacy against Gram-negative bacteria, particularly *E. coli* (31.67 mm) and *H. influenzae* (30 mm) at the same concentration. PANI/CB composite treatment exhibited the highest overall antimicrobial activity, especially against *E. coli* (32.33 mm) and *H. influenzae* (31.33 mm) at 1000 µg mL^{-1}, suggesting it might be the most effective broad-spectrum antimicrobial agent among the three treatments. The differential effectiveness against Gram-positive and Gram-negative bacteria among the treatments suggests potential complementary use in therapeutic applications. The investigated materials may be a good substitute for conventional antibiotics in the fight against bacterial resistance.

3.2.2. The antifungal activity. The CB, PANI, and their composite were used in the fungal broth microdilution test. Many research has examined how nanomaterials interact with fungi, but very few have looked into how they affect fungi. The

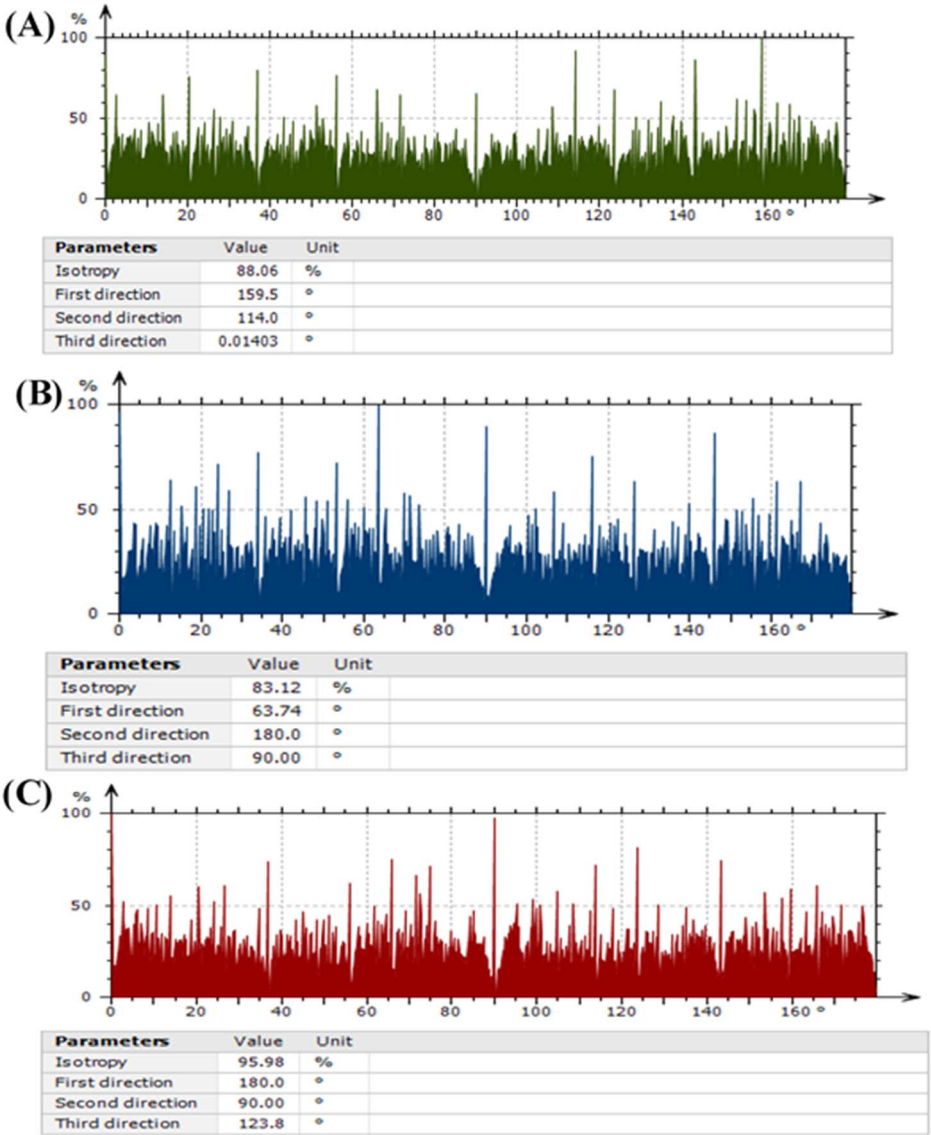

Fig. 7 Cartesian graphs of the surface texture directions for (A) PANI, (B) CB, and (C) PANI/CB.

Table 2 Textural characteristics of three samples

	Values of parameters		
Parameters	PANI	CB	PANI/CB
Total roughness (R_t) (nm)	52.12	0.63	170.00
Fractal dimension (D_f)	1.170	1.418	1.109
Slope	0.996	0.998	0.998
Roughness skewness (R_{sk})	0.218	−0.587	0.303
Roughness kurtosis (R_{ku})	1.881	2.916	2.608

MICs of all the tested isolates were similar to the MFCs, as shown in Fig. 9, indicating the fungicidal activity of the composite. The MFC for composite showed fungicidal activity as shown in Fig. 9.

An experiment with sorbitol was conducted, repeated, and quantified in order to assess the antifungal activity of the tested nanomaterial (mechanism of action of PANI, CB, and composite nanoparticles as an antifungal agent). To clarify the distinct mechanism of action of the studied drugs against various fungal strains, the MIC data were repeated on different sorbitol media, since a lower effective MIC is indicated of no effect on the fungal cell wall but probably by affecting another target. PANI, CB, and their composite were more active at dosages of 62 and 85 μg mL^{-1} against *P. notatum*, *M. indicus*, and *A. fumigatus*. as demonstrated in Fig. 10. The MFC results utilizing a different medium with extra sorbitol concentrations showed lower fungicidal concentrations against the same species in addition to reduced effective fungicidal concentrations against *Mucor* and *Penicillium*. *Penicillium* and *Mucor*'s MFC concentrations reduced to 62 and 85 μg mL^{-1}, respectively, as shown in Fig. 10.

About the antifungal activity through the zone of inhibition; regarded as one of the most precise techniques for determining antifungal or antibacterial activity is the disc diffusion

Table 3 Biological MIC and MBC (μg ml^{-1}) tests evaluated for PANI, CB, and PANI/CB nanocomposite against different bacterial strains

	PANI		CB		PANI/CB		Standard	
Microorganism	MIC	MBC	MIC	MBC	MIC	MBC	MIC	MBC
Staphylococcus aureus	27.33 ± 8	55 ± 15.55	0.66 ± 0.288	1.33 ± 0.57	16	16	16	32
Streptococcus pneumoniae	53.66 ± 14.6	107.33 ± 29.22	0.833 ± 0.208	1.66 ± 0.57	21.67 ± 8	446.66 ± 15.55	16	32
Listeria monocytogenes	125	125	6.66 ± 1.88	10 ± 5.29	32	66	16	32
Haemophilus influenzae	16	16	250	500	8	8	4	8
Bacillus subtilis	84.33 ± 28.75	166.66 ± 58.92	16	32	66	66	8	16
Escherichia coli	6.66 ± 1.88	6.66 ± 1.88	500	500	6.66 ± 1.88	6.66 ± 1.88	8	16

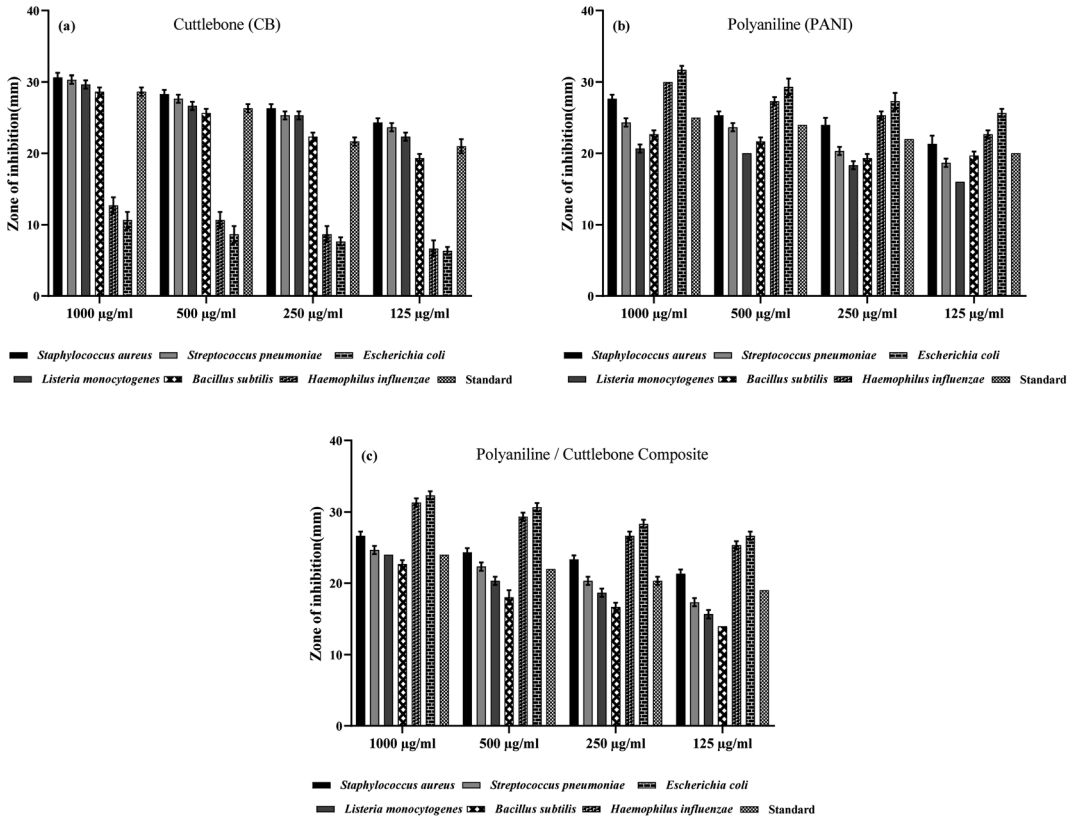

Fig. 8 The calculated inhibition zone mean (mm) against a variety of bacterial species at different concentrations of (a) CB, (b) PANI, and (c) composites (mean ± SE) against standard antibiotics (doxycycline for both Gram-positive and Gram-negative bacteria) as shown. The PANI and CB composites were the best wider and larger obtained zones of inhibition in mm.

technique. Inhibitory zones against different fungal strains were assessed on SDA plates; different doses are shown in Fig. 11. Compared to chlorohexidine, a typical antifungal for rapidly growing fungus, PANI, CB, and composite nanoparticles showed a good zone of inhibition against *Aspergillus*, *penicillium*, and *Candida* at 1000, 500, and 250 μg mL^{-1}. All the tested materials demonstrated good antifungal activity against the other fungal strains, as shown in Fig. 11.

Concerning antifungal activity (percentage of inhibition), following the addition of materials to the medium, the evaluation of antifungal activity was used to compute the percentage of fungal inhibition, which is displayed in Fig. 12. *Mucor indicus* was inhibited by PANI, CB, and composite nanoparticles at a rate of 73%, whereas *Candida albicans* was inhibited at a rate of 71%. The distinct features of CB, PANI, and composite nanoparticles—such as their uniform dispersion, broad surface area, and compact size—are what give them their antifungal action. The highest inhibitory percentage against isolates of *A. fumigates* is 80%.

The current investigation has found that powdered cuttlebone exhibits antimicrobial properties, likely due to the presence of polysaccharides like chitosan and inorganic substances such as $CaCO_3$ in its chemical composition. Chitosan, a natural polymer, has been shown to effectively combat various strains of bacteria,[40] including both Gram-positive and Gram-negative types. It has been proven to be effective against pathogens such as *Staphylococcus aureus*, *Staphylococcus epidermidis*, *Bacillus cereus*, *Bacillus megaterium*, *Listeria monocytogenes*,

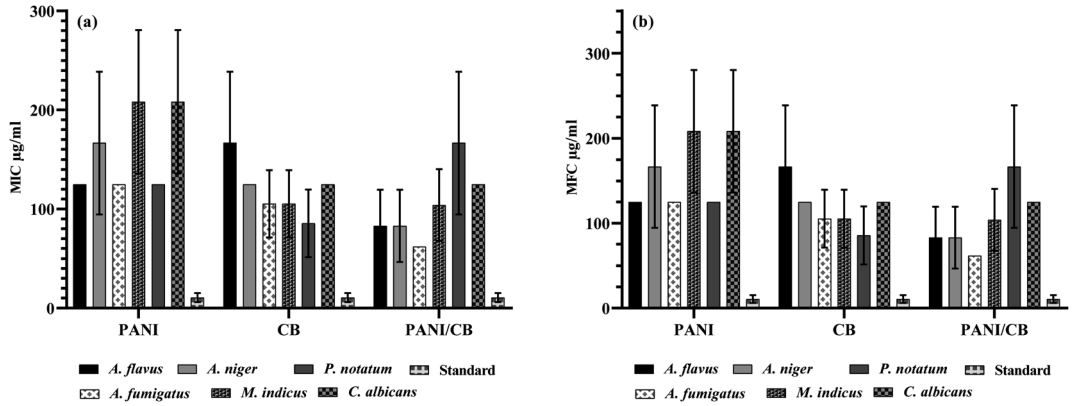

Fig. 9 Presents (a) MIC (µg mL^{-1}), and (b) MFC (µg mL^{-1}) values of PANI, CB, and composite nanoparticles without sorbitol against tested fungal isolates in triplicates (mean ± SE). The best MFC obtained was against *A. fumigatus* followed by *niger* and *flavus* while *Mucor* and *Candida* isolate one are of higher concentration as shown.

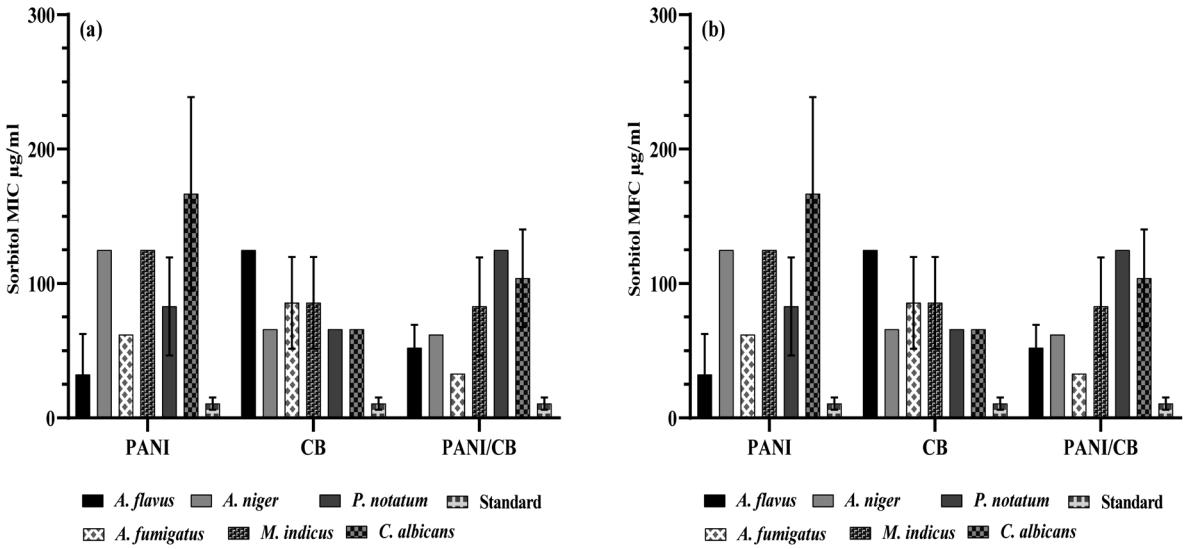

Fig. 10 Presents (a) the MIC (µg mL^{-1}), and (b) MFC (µg mL^{-1}) values in the presence of sorbitol of PANI, CB, and composite nanoparticles against tested fungal isolates in triplicates (mean ± SE). The best MIC obtained was against *A. fumigatus* followed by *flavus* and *niger* while *Candida* and *Mucor* isolates one are of higher concentration as showed. Lower MIC after adding of sorbitol in media with fungi indicates the materials mechanism of action not act mainly on cell wall but affecting another target.

Lactobacillus brevis, *Escherichia coli*, *Pseudomonas aeruginosa*, *Pseudomonas fluorescens*, and *Salmonella typhimurium*.[41] Extensive research has been conducted to understand the antibacterial mechanism of chitosan and its derivatives, but it remains incompletely understood. It is believed that the mechanism may differ between Gram-positive and Gram-negative bacteria due to differences in their cell surface properties.[42] Notably, Gram-negative bacteria are more susceptible to chitosan and its derivatives due to their higher negative charge on the cell surface.[43,44] The electrostatic interactions between the positively charged chitosan and the negatively charged bacterial cell surface are crucial to its antibacterial activity. This interaction leads to structural changes in the cell wall (Gram-positive) or outer membrane (Gram-negative), disrupting the permeability of the cytoplasmic membrane and causing leakage of essential cellular components like enzymes, nucleotides, and ions, ultimately resulting in bacterial cell death.[40,43,45] Other proposed mechanisms of action include the molecular weight and physical form of chitosan. Low molecular weight chitosan, whether in water-soluble form or as small nanoparticles, can penetrate the cell wall and inhibit mRNA synthesis and DNA transcription[42] On the other hand, high molecular weight chitosan and larger nanoparticles may create a barrier on the cell surface, hindering the transport of essential nutrients into the bacterial cell. Chitosan may also chelate metal cations and essential nutrients necessary for bacterial growth, further contributing to its antibacterial properties.[42] In addition to chitosan, the antimicrobial effectiveness of cuttlebone is enhanced by the presence of calcium oxide (CaO). The antibacterial properties of CaO nanoparticles (NPs) are demonstrated through their interaction with the bacterial cell membrane, causing disruption and leakage of cell contents. Additionally, CaO NPs release calcium

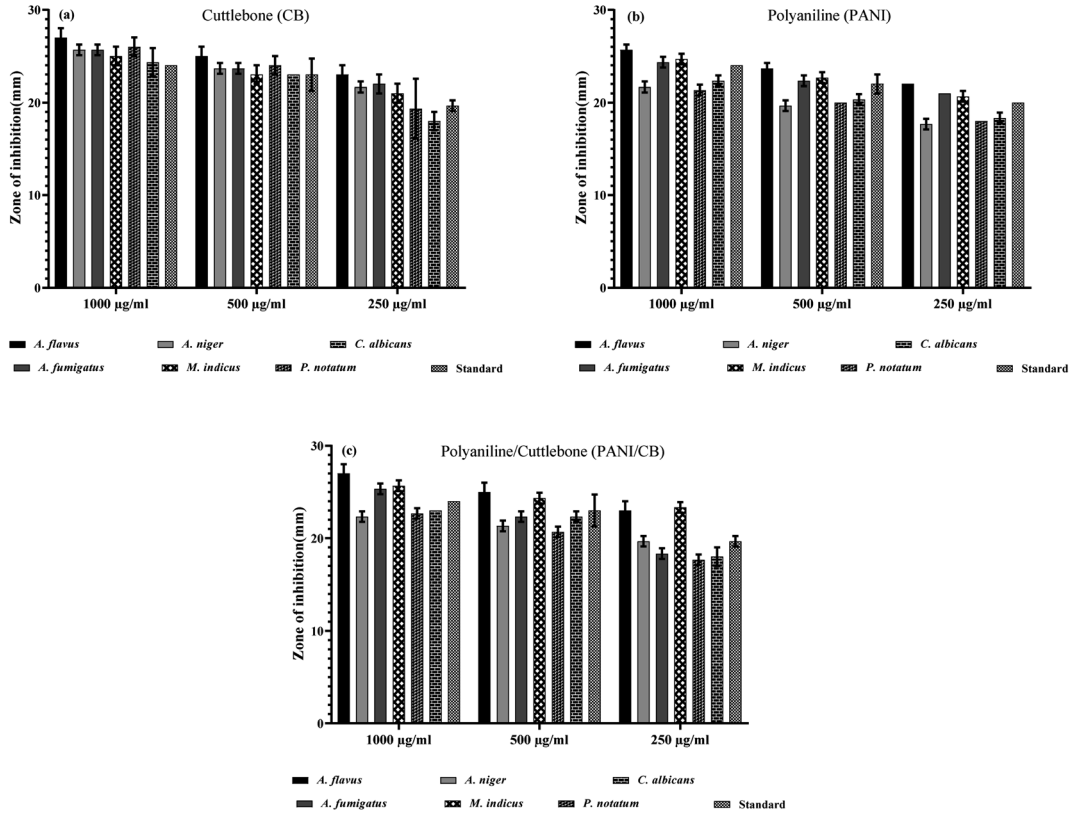

Fig. 11 The calculated inhibition zone mean (mm) against a variety of fungal isolates at different concentrations of (a) CB, (b) PANI, and (c) composites (mean ± SE) against standard antifungal agent cyclohexamide. The PANI and CB composites were the best wider and larger obtained zones of inhibition in mm.

ions (Ca^{2+}) and hydroxide ions (OH), which increase the pH and can disrupt bacterial cellular processes, ultimately leading to the bacteria's death. Furthermore, CaO NPs have the ability to produce reactive oxygen species, which can induce oxidative stress and ultimately result in the death of bacterial cells.[46]

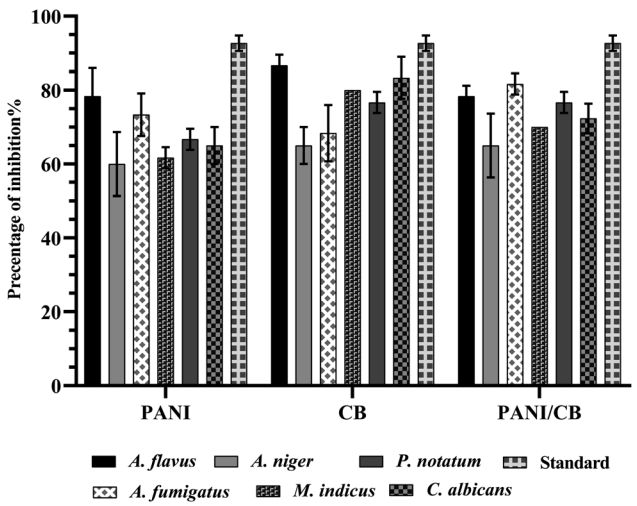

Fig. 12 Percentage of inhibition (%) against several fungal strains in SDA media. Cuttlebone showed higher antifungal inhibitory percentages, especially against *A. flavus* and *Candida albicans*.

Furthermore, minute quantities of zirconium oxide present in cuttlebone play a role in enhancing its antimicrobial characteristics. The mechanism behind the antibacterial efficacy of ZrO_2 Nps involves the generation of reactive oxygen species, causing modifications in membrane permeability that result in the excretion of lipids and proteins, ultimately culminating in microbial cell death[47]

On the contrary, the antimicrobial properties exhibited by PANI stem from its unique structural composition containing amino and hydrocarbon groups. PANI entities are characterized by numerous cationic charges,[48] whereas the external layer of bacterial cells carries an anionic charge. This phenomenon is facilitated by the presence of teichoic (or lipoteichoic) acid components within the cell envelope of Gram-positive bacteria, as well as lipopolysaccharides and phospholipids present in the outer membrane of Gram-negative bacteria, and the cytoplasmic membrane (CPM) itself, which is composed of a phospholipid bilayer housing essential integral proteins like enzymes.[49–51] The interaction between polycations and cellular membranes leads to the integration of hydrophobic hydrocarbon groups of the polymer into the cell plasma membrane (CPM). These alterations result in structural disarray and compromise the integrity of cellular membranes, ultimately causing CPM disintegration, cytoplasmic content leakage, cell lysis,[52] and/or hindrance of membrane-associated processes such as nutrient transport and cellular respiration,

consequently impeding the proliferation of microorganisms.[53] PANI may potentially exert its effects through other mechanisms, such as upregulating the expression of oxidative damage-responsive genes, downregulating genes related to energy metabolism, transport, and cell wall synthesis, and possibly impacting the development of stress-resistant biofilms.[54] Moreover, PANI has also been observed to generate hydrogen peroxide, a substance that has the ability to facilitate the creation of hydroxyl radicals, resulting in harm to biomolecules and potentially leading to cellular death.[55] The synergistic effect observed when polyaniline is combined with cuttlebone leads to an enhancement in the overall antimicrobial activity. This enhancement may be attributed to the distinctive structural and chemical properties inherent in each component, as previously discussed.

3.3. Cytotoxicity evaluation of in Huh-7 cells

The MTT assay results for Huh7 cells after treatment with PANI, CB, PANI/CB, DOX, and DOX + PANI/CB demonstrate varying degrees of cytotoxicity across different concentrations (7.8 to 1000 μg mL^{-1}). Both PANI and CB treatments show minimal cytotoxic effects, with cell viability remaining above 80% at all concentrations, indicating that these materials alone are relatively non-toxic to Huh7 cells. The PANI/CB combination exhibits slightly increased cytotoxicity compared to the individual components, but cell viability remains above 60%, even at the highest concentration. In contrast, DOX shows a clear dose-dependent reduction in cell viability, with significant cytotoxicity observed at higher concentrations (500 and 1000 μg mL^{-1}), reducing cell viability to around 50%. Notably, the combination of DOX with PANI/CB further enhances the cytotoxic effect, resulting in a more pronounced decrease in cell viability compared to DOX alone, particularly at higher concentrations where viability drops below 50%. These results suggest that while PANI and CB are biocompatible on their own, their combination with DOX enhances the drug's anticancer efficacy through a potential synergistic effect, making the PANI/CB composite a promising candidate for drug delivery applications as shown in Fig. 13.

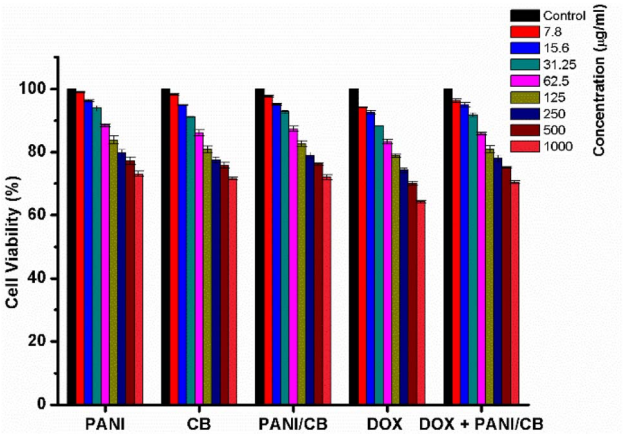

Fig. 13 Cell viability (%) of PANI, CB, PANI/CB, Dox, and Dox + PANI/CB at different concentrations after 24 h, ($n = 3$) ± SD.

3.4. Serum analysis of ALT, AST, creatinine, and urea determination

The levels of urea and creatinine in the serum were altered after treatment with PANI, CB, and composite following Dox injection. However, the administration of Dox significantly increased the concentrations of urea and creatinine compared to the normal group. Treatment with PANI, CB and composite reduced the DOX-induced increase in renal function tests, as shown in Table 4. On the other hand, after two weeks of DOX injections, there was a significant increase in serum ALT and AST activities. However, when DOX-injected rats were supplemented with PANI, there was a significant reduction in elevated serum AST and ALT activities. Similarly, supplementation with cuttlebone also led to a significant reduction in elevated serum AST and ALT activities. Additionally, supplementation with a combination of polyaniline and cuttlebone (composite) resulted in a significant reduction in elevated serum AST and ALT activities (Table 5).

DOX is a widely used and highly potent chemotherapeutic agent. However, its application is significantly limited due to the risk of multi-organ toxicity.[56] The renal and hepatic systems are particularly vulnerable to DOX due to their roles in drug metabolism and excretion. As a result, DOX tends to accumulate preferentially in these organs after systemic administration.[57] Elevated levels of urea and creatinine indicate renal impairment, while increased levels of alanine aminotransferase (ALT) and aspartate aminotransferase (AST) suggest hepatic injury. Studies have shown that incorporating PANI, CB, and PANI/CB nanocomposites can effectively reduce DOX-induced elevations in urea, creatinine, ALT, and AST, indicating a protective or therapeutic impact on renal and hepatic functions. Supplementation of DOX-injected rats with these materials leads to a significant decrease in the elevated levels of AST, ALT, urea, and creatinine. PANI and CB, particularly their chitosan and polysaccharide constituents, are known for their antioxidant properties, which can neutralize reactive oxygen species (ROS) produced by doxorubicin and alleviate tissue damage. Studies have shown that PANI can efficiently scavenge free radicals, as demonstrated by the DPPH assay. The antioxidant efficacy of PANI is dependent on the morphology and composition of PANI/CB nanocomposites.[58] Investigations have also revealed that chitosan extracted from cuttlebone has a concentration-dependent ability to neutralize free radicals, with reported scavenging activities of 59.7% for DPPH radicals and 56% for

Table 4 Impact of PANI, CB, and PANI/CB on the elevation of serum urea and creatinine levels induced by doxorubicin

	Serum	
Treatment	Urea (mg dL^{-1})	Creatinine (mg dL^{-1})
Control	33.6 ± 1.4	0.7 ± 0.01
Doxorubicin	86 ± 1.4	1.05 ± 0.03
DOX + PANI	40.3 ± 0.4	0.9 ± 0.02
DOX + CB	43.6 ± 2.6	0.9 ± 0.007
DOX + PANI/CB	39 ± 0.7	0.53 ± 0.01

Table 5 The impact of PANI, CB, and the PANI/CB composite on the elevation of serum alanine aminotransferase (ALT) and aspartate aminotransferase (AST) levels induced by doxorubicin

	Serum	
Treatment	ALT (IU L^{-1})	AST (IU L^{-1})
Control	41 ± 0.7	25 ± 0.4
Doxorubicin	48 ± 2.8	195 ± 0.7
DOX + PANI	30 ± 0.4	148.6 ± 1.6
DOX + CB	33 ± 0.7	92.3 ± 1.4
DOX + PANI/CB	21 ± 0.4	13 ± 1.08

hydrogen peroxide at designated concentrations.[59] Furthermore, polysaccharides isolated from cuttlebone have demonstrated comparable antioxidant capabilities, achieving scavenging activity of up to 74.36%. These compounds also possess chelating characteristics towards ferrous ions, which helps inhibit the Fenton reaction and the production of harmful hydroxyl radicals, further enhancing their antioxidant efficacy.[60] The synergistic combination of PANI and CB may improve the properties and stability of the synthesized nanocomposite, thereby amplifying its protective effects against the toxicity associated with DOX.

4 Conclusion

In conclusion, this research demonstrates the significant potential of utilizing cuttlebone waste as a sustainable and eco-friendly resource for the development of antimicrobial materials. The study highlights the effective use of cuttlebone as a bioactive agent and a supporting phase for polyaniline, resulting in a potent nanocomposite with good antibacterial and antifungal properties. The combination of PANI/CB with DOX effectively enhances cytotoxicity against Huh7 cells compared to DOX alone, indicating the potential of PANI/CB as a promising drug delivery system to boost chemotherapeutic outcomes. Additionally, the protective efficacy of the PANI/CB nanocomposite against DOX-induced hepatic and renal injury in rats was demonstrated through significant improvements in liver and kidney function markers. Treatment with the nanocomposite markedly reduced serum ALT levels from 48 ± 2.8 IU L^{-1} to 21 ± 0.4 IU L^{-1}, AST from 195 ± 0.7 IU L^{-1} to 13 ± 1.08 IU L^{-1}, urea from 86 ± 1.4 mg dL^{-1} to 39 ± 0.7 mg dL^{-1}, and creatinine from 1.05 ± 0.03 mg dL^{-1} to 0.53 ± 0.01 mg dL^{-1}, indicating its ability to mitigate oxidative damage. This study emphasizes the importance of utilizing waste materials like cuttlebone not only for environmental benefits, but also for their functional properties in enhancing the efficacy of antimicrobial agents. This innovative approach not only addresses waste management issues, but also contributes to the development of novel and effective antimicrobial therapies, opening new avenues for research and application in combating infectious diseases. The promising results encourage further exploration into the use of natural and waste-derived materials in the creation of advanced biomedical and environmental solutions.

Future perspective

Studying the impact on DOX efficacy would be crucial for a complete understanding of the PANI/CB–DOX interaction. This could be addressed through investigation of tumor response in the presence of PANI/CB–DOX combination. Analysis of DOX pharmacokinetics when administered with PANI/CB. Evaluation of cancer cell death rates and mechanisms in the presence of both compounds. Evaluating tumor growth inhibition in animal models treated with the combination to determine any synergistic or antagonistic effects on doxorubicin's anticancer activity. Investigating potential changes in drug uptake and distribution within tumor tissues when combined with PANI/CB. These studies would provide a comprehensive assessment of both the protective effects and potential impact on therapeutic efficacy.

Data availability

The datasets used and/or analyzed during the current study are available from the corresponding author upon reasonable request.

Conflicts of interest

The authors declare no conflicts of interest.

Acknowledgements

This study/publication was made possible by the generous support of the American people through the United States Agency for International Development (USAID). The contents are the responsibility of [Esraa Salama] and do not necessarily reflect the views of USAID or the United States Government. In addition, this study/publication (Project ID: Tailored Enzymatic and Nano-Based Treatment of Wastewater to Detoxify Heavy Metals and Degrade Antibiotics) was made possible by the generous support of the American people through the United States Agency for International Development (USAID). The contents are the responsibility of [Hamdaa Mahmoud] and do not necessarily reflect the views of USAID or the United States Government.

References

1 J. Kubar and K. Fragaki, Recombinant DNA-derived leishmania proteins: from the laboratory to the field, *Lancet Infect. Dis.*, 2005, **5**, 107–114.
2 J. B. Calixto, The role of natural products in modern drug discovery, *An. Acad. Bras. Cienc.*, 2019, **91**, 1–7.
3 M. L. Cohen, Epidemiology of drug resistance: implications for a post-antimicrobial era, *Science*, 1992, **257**, 1050–1055.
4 P. Koehler, D. Tacke and O. A. Cornely, Aspergillosis of bones and joints–a review from 2002 until today, *Mycoses*, 2014, **57**, 323–335.
5 S. M. Swain, F. S. Whaley and M. S. Ewer, Congestive heart failure in patients treated with doxorubicin: a retrospective analysis of three trials, *Cancer*, 2003, **97**, 2869–2879.

6 V. D'Agati and A. M. Schmidt, RAGE and the pathogenesis of chronic kidney disease, *Nat. Rev. Nephrol.*, 2010, **6**, 352–360.
7 S. Harbarth, H. H. Balkhy, H. Goossens, V. Jarlier, J. Kluytmans, R. Laxminarayan, M. Saam, A. Van Belkum, D. Pittet and World Healthcare-Associated Infections Resistance Forum participants, Antimicrobial resistance: one world, one fight, *Antimicrob. Resist. Infect. Control*, 2015, **4**(49), 1–15.
8 P. D. Gupta and T. J. Birdi, Development of botanicals to combat antibiotic resistance, *J. Ayurveda Integr. Med.*, 2017, **8**, 266–275.
9 J. Guarro, J. Gené and A. M. Stchigel, Developments in fungal taxonomy, *Clin. Microbiol. Rev.*, 1999, **12**, 454–500.
10 Y. Zhang, F. Hagen, B. Stielow, A. M. Rodrigues, K. Samerpitak, X. Zhou, P. Feng, L. Yang, M. Chen, S. Deng, S. Li, W. Liao, R. Li, F. Li, J. F. Meis, J. Guarro, M. Teixeira, H. S. Al-Zahrani, Z. de Camargo, L. Zhang and G. S. de Hoog, Phylogeography and evolutionary patterns in Sporothrix spanning more than 14 000 human and animal case reports, *Pers.: Mol. Phylogeny Evol. Fungi*, 2015, **35**, 1–20.
11 I. Algoritma, A. Untuk, M. T. Penjualan, P. Store, A. Aeon and D. Dermawan, *Implementasi algoritma apriori untuk menentukan tingkat penjualan pada store adidas aeon sentul*, 2023, pp. 1–14.
12 R. S. Diggikar, S. P. Deshmukh, T. S. Thopate and S. R. Kshirsagar, Performance of Polyaniline Nanofibers (PANI NFs) as PANI NFs-Silver (Ag) Nanocomposites (NCs) for Energy Storage and Antibacterial Applications, *ACS Omega*, 2019, **4**, 5741–5749.
13 J. Hermelin, J. Diaz, R. D. Thilaga and V. Sivakumar, In-Vitro Cytotoxic Activity of Squid and Cuttlefish Bone Extract on Hep G2 Cell Line, *Int. J. Pharma Sci. Res.*, 2015, **6**, 778–782.
14 R. Hongsathavij and K. R. Yosvimol Kuphasuk, Effectiveness of platelet-rich fibrin in the management of pain and delayed wound healing, *Eur. J. Dent.*, 2017, **11**, 192–195.
15 M. H. Azarian and W. Sutapun, Biogenic calcium carbonate derived from waste shells for advanced material applications: a review, *Front. Mater.*, 2022, **9**, 1–17.
16 N. Suwannasingha, A. Kantavong, S. Tunkijjanukij, C. Aenglong, H. B. Liu and W. Klaypradit, Effect of calcination temperature on structure and characteristics of calcium oxide powder derived from marine shell waste, *J. Saudi Chem. Soc.*, 2022, **26**, 101441.
17 G. Montes-Atenas and F. Valenzuela, Wastewater Treatment through Low Cost Adsorption Technologies, *Physico-Chemical Wastewater Treatment and Resource Recovery*, 2017, pp. 213–238.
18 M. E. Ernst, M. E. Klepser, E. J. Wolfe and M. A. Pfaller, Antifungal dynamics of LY 303366, an investigational Echinocandin B analog, against Candida ssp, *Diagn. Microbiol. Infect. Dis.*, 1996, **26**, 125–131.
19 A. Espinel-Ingroff, V. Chaturvedi, A. Fothergill and M. G. Rinaldi, Optimal testing conditions for determining MICs and minimum fungicidal concentrations of new and established antifungal agents for uncommon molds: NCCLS collaborative study, *J. Clin. Microbiol.*, 2002, **40**, 3776–3781.
20 I. L. Fibrosis, O. Stress, N. Aljobaily, M. J. Viereckl, D. S. Hydock, H. Aljobaily, T. Wu, R. Busekrus, B. Jones, J. Alberson and Y. Han, Creatine alleviates doxorubicin-induced liver damage by inhibiting liver fibrosis, inflammation, oxidative stress, and cellular senescence, *Nutrients*, 2020, **13**(1), 41.
21 A. F. Wali, S. Rashid, S. M. Rashid, M. A. Ansari, M. R. Khan, N. Haq and M. U. Rehman, Naringenin regulates doxorubicin-induced liver dysfunction: impact on oxidative stress and inflammation, *Plants*, 2020, **9**(4), 550.
22 H. An, Y. Wang, X. Wang, N. Li and L. Zheng, The preparation of PANI/CA composite electrode material for supercapacitors and its electrochemical performance, *J. Solid State Electrochem.*, 2010, **14**, 651–657.
23 Q. B. Le, T. H. Nguyen, H. Fei, I. Sapurina, F. A. Ngwabebhoh, C. Bubulinca, L. Munster, E. D. Bergerová, A. Lengalova, H. Jiang, T. D. Tran, N. Bugarova, M. Omastova, N. E. Kazantseva and P. Saha, Electrochemical performance of composites made of rGO with Zn-MOF and PANI as electrodes for supercapacitors, *Electrochim. Acta*, 2020, 137563.
24 K. Lee, S. Cho, M. Kim, J. Kim, J. Ryu, K. Y. Shin and J. Jang, Highly porous nanostructured polyaniline/carbon nanodots as efficient counter electrodes for Pt-free dye-sensitized solar cells, *J. Mater. Chem. A*, 2015, **3**, 19018–19026.
25 K. Periasamy and G. C. Mohankumar, Sea coral-derived cuttlebone reinforced epoxy composites: characterization and tensile properties evaluation with mathematical models, *J. Compos. Mater.*, 2016, **50**, 807–823.
26 B. M. Tyson, R. K. Abu Al-Rub, A. Yazdanbakhsh and Z. Grasley, A quantitative method for analyzing the dispersion and agglomeration of nano-particles in composite materials, *Composites, Part B*, 2011, **42**, 1395–1403.
27 M. Maruthapandi, V. B. Kumar, J. H. T. Luong and A. Gedanken, Kinetics, isotherm, and thermodynamic studies of methylene blue adsorption on polyaniline and polypyrrole macro–nanoparticles synthesized by C-dot-initiated polymerization, *ACS Omega*, 2018, **3**, 7196–7203.
28 S. Balu, M. V. Sundaradoss, S. Andra and J. Jeevanandam, Facile biogenic fabrication of hydroxyapatite nanorods using cuttlefish bone and their bactericidal and biocompatibility study, *Beilstein J. Nanotechnol.*, 2020, **11**, 285–295.
29 N. Nouj, N. Hafid, N. El Alem, I. I. Buciscanu, S. S. Maier, P. Samoila, G. Soreanu, I. Cretescu and C. D. Stan, Valorization of β-Chitin Extraction Byproduct from Cuttlefish Bone and Its Application in Food Wastewater Treatment, *Materials*, 2022, **15**, 2803.
30 K. Sankar and A. Achary, Bio-ceramic, mesoporous cuttlebone of Sepia officinalis is an ideal support for the immobilization of Bacillus subtilis AKL13 lipase: optimization, adsorption, thermodynamic and reaction kinetic studies, *Chem. Pap.*, 2020, **74**, 459–470.
31 S. Senthilkumar and A. Rajendran, Synthesis, Characterization and Electrical Properties of Nano Metal and Metal-Oxide Doped with Conducting Polymer

Composites by in-Situ Chemical Polymerization, *MOJ Polym. Sci.*, 2017, **1**(31), 1–4.
32 A. Dutta, S. Fermani, S. Arjun Tekalur, A. Vanderberg and G. Falini, Calcium phosphate scaffold from biogenic calcium carbonate by fast ambient condition reactions, *J. Cryst. Growth*, 2011, **336**, 50–55.
33 M. H. Suhail, O. G. Abdullah and G. A. Kadhim, Hydrogen sulfide sensors based on PANI/f-SWCNT polymer nanocomposite thin films prepared by electrochemical polymerization, *J. Sci.: Adv. Mater. Devices*, 2019, **4**, 143–149.
34 S. Vijayalakshmi, E. Kumar, M. Ganeshbabu, P. S. Venkatesh and K. Rathnakumar, Structural, electrical, and photocatalytic investigations of PANI/ZnO nanocomposites, *Ionics*, 2021, **27**, 2967–2977.
35 N. Sirotkin and A. Khlyustova, Plasma Synthesis and Characterization of PANI+ WO3 Nanocomposites and their Supercapacitor Applications, *J. Compos. Sci.*, 2023, **7**, 174.
36 A. W. Burton, K. Ong, T. Rea and I. Y. Chan, On the estimation of average crystallite size of zeolites from the Scherrer equation: a critical evaluation of its application to zeolites with one-dimensional pore systems, *Microporous Mesoporous Mater.*, 2009, **117**, 75–90.
37 S. Khasim, Polyaniline-Graphene nanoplatelet composite films with improved conductivity for high performance X-band microwave shielding applications, *Results Phys.*, 2019, **12**, 1073–1081.
38 Ş. Ţălu, D. P. Shcherbinin, E. A. Konshina and I. A. Gladskikh, Stereometric and fractal analysis of granulated silver films used in thin-film hybrid structures, *J. Microsc.*, 2021, **281**, 46–56.
39 Ş. Ţălu, K. Janus and S. Stach, Nanoscale patterns in carbon – nickel nanocomposite thin films investigated by AFM and stereometric analysis, *Int. J. Mater.*, 2017, **4**, 54–62.
40 P. Zou, X. Yang, J. Wang, Y. Li, H. Yu, Y. Zhang and G. Liu, Advances in characterisation and biological activities of chitosan and chitosan oligosaccharides, *Food Chem.*, 2016, **190**, 1174–1181.
41 D. H. Ngo, T. S. Vo, D. N. Ngo, K. H. Kang, J. Y. Je, H. N. D. Pham and S. K. Kim, Biological effects of chitosan and its derivatives, *Food Hydrocoll.*, 2015, **51**, 200–216.
42 M. A. Matica, F. L. Aachmann, A. Tøndervik, H. Sletta and V. Ostafe, Chitosan as a wound dressing starting material: antimicrobial properties and mode of action, *Int. J. Mol. Sci.*, 2019, **20**, 1–33.
43 I. Younes and M. Rinaudo, Chitin and chitosan preparation from marine sources. Structure, properties and applications, *Mar. Drugs*, 2015, **13**, 1133–1174.
44 M. Kong, X. G. Chen, K. Xing and H. J. Park, Antimicrobial properties of chitosan and mode of action: a state of the art review, *Int. J. Food Microbiol.*, 2010, **144**, 51–63.
45 Y. C. Chung and C. Y. Chen, Antibacterial characteristics and activity of acid-soluble chitosan, *Bioresour. Technol.*, 2008, **99**, 2806–2814.
46 A. U. Khan, T. Hussain, S. Abdullah, M. A. Khan, M. M. Almostafa, N. S. Younis and G. Yahya, Antibacterial and Antibiofilm Activity of Ficus carica-Mediated Calcium Oxide (CaONPs) Phyto-Nanoparticles, *Molecules*, 2023, **28**, 1–13.
47 L. S. R. Yadav, B. M. Shilpa, B. P. Suma, R. Venkatesh and G. Nagaraju, Synergistic effect of photocatalytic, antibacterial and electrochemical activities on biosynthesized zirconium oxide nanoparticles, *Eur. Phys. J. Plus*, 2021, **136**, 1–17.
48 Z. A. Boeva and V. G. Sergeyev, Polyaniline: Synthesis, Properties, and Application, *Polym. Sci. Ser. C*, 2014, **56**, 144–153.
49 P. Gilbert and L. E. Moore, Cationic antiseptics: diversity of action under a common epithet, *J. Appl. Microbiol.*, 2005, **99**, 703–715.
50 L. Timofeeva and N. Kleshcheva, Antimicrobial polymers: mechanism of action, factors of activity, and applications, *Appl. Microbiol. Biotechnol.*, 2011, **89**, 475–492.
51 A. N. Andriianova, L. R. Latypova, L. Y. Vasilova and A. G. Mustafin, Antibacterial properties of polyaniline derivatives, *J. Appl. Polym. Sci.*, 2021, **138**, 1–11.
52 G. J. Gabriel, J. A. Maegerlein, C. F. Nelson, J. M. Dabkowski, T. Eren, K. Nüsslein and G. N. Tew, Comparison of Facially Amphiphilic versus Segregated Monomers in the Design of Antibacterial Copolymers, *Chem.–A Eur. J.*, 2009, **15**, 433–439.
53 P. Shaklee, M. Kostic, J. Chataway, M. Keynes and A. Colman, Editorial Board, *Trends Biotechnol.*, 2011, **29**, 419–472.
54 M. R. Gizdavic-nikolaidis, J. R. Bennett, S. Swift, A. J. Easteal and M. Ambrose, Acta biomaterialia broad spectrum antimicrobial activity of functionalized polyanilines, *Acta Biomater.*, 2011, **7**, 4204–4209.
55 J. Robertson, M. Gizdavic-nikolaidis and M. K. Nieuwoudt, The antimicrobial action of polyaniline involves production of oxidative stress while functionalisation of polyaniline introduces additional mechanisms, *PeerJ*, 2018, **6**, 1–36.
56 A. J. Smuder, Exercise stimulates beneficial adaptations to diminish doxorubicin-induced cellular toxicity, *Am. J. Physiol. Regul. Integr. Comp. Physiol.*, 2024, **317**, 662–672.
57 L. Francisco, M. Locci, D. Oliveira, A. Rocha, J. Moreira, D. Andrade and V. Lucia, Journal of pharmaceutical and biomedical analysis total, renal and hepatic clearances of doxorubicin and formation clearance of doxorubicinol in patients with breast cancer: estimation of doxorubicin hepatic extraction ratio, *J. Pharm. Biomed. Anal.*, 2020, **185**, 113231.
58 F. N. Pur, N. Arsalani and K. D. Safa, Novel Free-Radical Scavengers Based On Ferrofluid/Polyaniline Nanocomposites, *Pharm. Chem. J.*, 2018, **51**, 1138–1142.
59 R. Iberahim, N. Ibrahim, S. Aminah, S. Mohamad, R. Rusmin, N. A. Jailani, N. Illiya and Z. Zulkifli, Antioxidant and antimicrobial activity of cuttlebone chitosan against Escherichia coli, Staphylococcus aureus and Candida albicans, *Malaysian Applied Biology*, 2022, **51**, 103–108.
60 P. Ramasamy, N. Subhapradha and V. Shanmugam, Extraction, characterization and antioxidant property of chitosan from cuttlebone Sepia kobiensis (Hoyle 1885), *Int. J. Biol. Macromol.*, 2014, **64**, 202–212.